

1 **PFAS destruction and near complete defluorination of undiluted aqueous film-forming**
2 **foams at ambient conditions by piezoelectric ball milling**

3
4 Nanyang Yang,¹ Yunqiao Guan¹, Shasha Yang,^{1,2} Caitlyn Olive,¹ Sujan Fernando,¹ Thomas M.
5 Holsen,¹ Yang Yang^{1*}
6

7 ¹ Department of Civil and Environmental Engineering, Clarkson University, Potsdam, New York
8 13699, United States

9 ² Institute for a Sustainable Environment, Clarkson University, Potsdam, New York 13699, United
10 States

11 * Corresponding author: Email: yanyang@clarkson.edu; Tel: +1-315-268-3861
12

13 **ABSTRACT**

14 The non-thermal destruction of aqueous film-forming foam (AFFF) stockpiles, one of the major
15 culprits responsible for water and soil contamination by per- and polyfluoroalkyl substances
16 (PFAS), is extremely challenging because of the coexistence of mixed recalcitrant PFAS and
17 complicated organic matrices at extremely high concentrations. To date, the complete
18 defluorination of undiluted AFFF at ambient conditions has not been demonstrated. This study
19 reports a novel piezoelectric ball milling (BM) approach for treating AFFF with a total organic
20 fluorine concentration of 9,080 mg/L and total organic carbon of 234 g/L. Near-complete
21 defluorination (> 95% conversion of organofluorine to fluoride) of undiluted AFFF was achieved
22 by co-milling with boron nitride (BN). By carefully examining the experimental data, we identified
23 AFFF liquid film thickness (*Z*) at the collision interface as a descriptor of treatment performance.
24 We further validated that effective defluorination proceeded when *Z* was less than a criteria value
25 of 2.3 μm. In light of this new understanding, the addition of SiO₂ as a dispersant and the pre-
26 evaporation solvents to reduce *Z* have been validated as effective strategies to promote AFFF
27 treatment capacity.
28
29

30 Introduction

31 Per- and polyfluoroalkyl substances (PFAS) are synthetic chemicals used since the 1940s.¹ Their
32 ubiquitous presence in the environment, significant toxicity, and persistence have raised growing
33 public concerns.² Aqueous film-foaming foam (AFFF) was identified as the major culprit
34 responsible for the elevated PFAS concentration in the receiving water and soil of manufacturing
35 sites, airports, and military fire training areas.³⁻⁵

36 The most urgently needed proactive solution to curb new PFAS contamination from using
37 AFFF is the disposal of the existing chemical stockpile. The incineration of AFFF is facing
38 regulatory challenges due to concerns about the emission of incomplete combustion products and
39 greenhouse gas.^{6,7} Alternative non-thermal technologies enabling near-complete defluorination
40 (i.e., conversion of organofluorine on PFAS to fluoride (F⁻)), in addition to degradation of parent
41 PFAS compounds, are desired to meet the zero PFAS pollution goal.⁸ However, deep
42 defluorination of even a single type of PFAS is challenging. For instance, the maximum
43 defluorination efficiencies of treating perfluorooctane sulfonic acid (PFOS) by electrochemical
44 oxidation, UV-sulfite photoreduction, and alkaline-assisted heat treatment are below 80%.⁹⁻¹¹ The
45 deep defluorination of AFFF, a mixture of concentrated PFAS with co-existing solvents and
46 surfactants,^{12,13} is a next-level challenge that has been inadequately addressed.

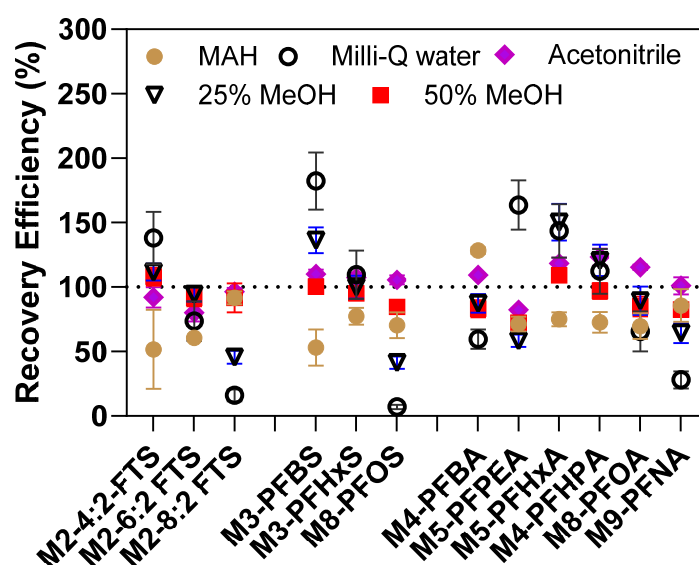
47 The past investigations of PFAS defluorination were heavily invested in the treatment of model
48 PFAS, with only a few studies that used electrochemical oxidation, plasma, advanced oxidation,
49 and UV-sulfite photoreduction to treat diluted AFFF with total fluorine (TF) ranging between 0.1-
50 27 mg F/L.¹³⁻¹⁷ All these technologies demonstrated structurally dependent reactivity in removing
51 target PFAS, and none achieved near-complete defluorination. To date, only hydrothermal alkaline
52 treatment realized ~100% defluorination of AFFF but demands high temperature (170-350°C),
53 pressurized reactors (2-22 MPa), and alkaline addition (5 M of NaOH).¹⁸

54 Ball milling (BM) is an emerging technology for destroying PFAS chemicals at ambient
55 conditions. Using potassium hydroxide (KOH) as a co-milling reagent destroys perfluorooctanoic
56 acid (PFOA) and perfluorooctane sulfonic acid (PFOS).^{19,20} However, the residual KOH in the
57 media must be neutralized before discharge. Using quartz sand (SiO₂) as a neutral reagent to
58 destroy PFAS is possible. However, the degradation kinetics are slower, and the fluoride yield is
59 low.^{20,21} Previously, we discovered that boron nitride (BN), a piezoelectric material, can be
60 activated in the BM process to generate ~kV potential to destroy solid PFAS.²² Building upon this

61 early success, this study reports unprecedented results that the BN-assisted BM (**BN-BM**) can
62 achieve ~100% defluorination of undiluted liquid AFFF with a TF concentration of $9,080 \pm 180$
63 mg/L (vs. 0.1-27 mg/L reported previously¹³⁻¹⁷). We further developed a critical liquid film theory
64 to guide the process scale-up. The critical insights of this study established a novel AFFF treatment
65 paradigm and expanded the applications of piezoelectric BM from solid chemical destruction to
66 liquid waste disposal.

67

68 **Comprehensive analytical approaches to close the fluorine balance.**



69

70 **Figure 1.** Comparison of the extraction recovery efficiencies of isotope-labelled PFAS using
71 various solvents. The prefix “M#” refers to the number of carbons labeled by ¹³C. An isotope-
72 labeled PFAS mixture (40 μ L of 1000 ng/mL for individual PFAS) was spiked in 100 mg BN.
73 Data are presented as means of triplicates \pm standard deviation.

74

75 This study developed a novel BN-BM process for the treatment of liquid AFFF. The AFFF was
76 found to contain 11 PFAS with different function groups and chain lengths and other unknown
77 fluorocarbons (Table S1; to be discussed in the following content). Therefore, it was critical to
78 identify a solvent that would ensure the effective extraction of all target PFAS from the milled
79 samples (slurry-like samples for AFFF treatment). To determine this, we spiked twelve isotope-
80 labeled PFAS (fluorocarbon number, n=3-9; each PFAS has a concentration of 1000 μ g/mL) into

81 the BN powder. The mixture was ultrasonically extracted using various solvents, including 0.3%
82 methanolic ammonium hydroxide (MAH; a solvent recommended by EPA Draft Method 1633²⁵),
83 Milli-Q water, 25% methanol (MeOH), 50% MeOH, and acetonitrile with 0.2% formic acid
84 (details are provided in [Text S1](#)). MeOH (50%) was the best-performing solvent, with recoveries
85 of PFAS with various structures from 80-110% ([Figure 1](#)).

86 Demonstrating the near-complete defluorination of individual PFAS and AFFF is the only
87 evidence that can be used to confirm PFAS mineralization and mitigated risk. In this study, the
88 PFAS destruction efficiency and degree of defluorination were based on the decay in PFAS
89 concentrations and the quantitative yield of F⁻ measured in extract solvents using both F⁻ and total
90 organic fluorine (TOF). The defluorination efficiency (**DeF**) was calculated as:

$$91 \quad \text{DeF (\%)} = ([F^-]_t - [F^-]_0) / ([TOF]_0 - [TOF]_t) \times 100\% \quad (1)$$

92 where [F⁻]₀ and [F⁻]_t are the molar mass of F⁻ in the extract solutions of samples before and after
93 BM treatment, respectively. [TOF]₀ and [TOF]_t are the molar mass of TOF before and after BM
94 treatment, respectively. For the destruction of analytical-grade PFAS chemicals, TOF is the
95 product of fluorine number and the parent PFAS concentration. The [TOF]₀ of AFFF was given
96 by the combination of CIC and IC analyses as described in the methods section. With the detection
97 limits of [F⁻] by IC of 50 µg/L, [TOF]_t down to the levels of nmol/L (based on targeted PFAS
98 analysis) and µmol/L (based on CIC measurements), the highly sensitive and comprehensive
99 analytical approaches were sufficient to determine if near-complete defluorination, arbitrarily
100 defined as DeF > 95% was achieved.

101

102 **Near-complete defluorination of individual PFAS.**

103 Using BN as a typical piezoelectric material, we demonstrated that piezoelectric BM achieved
104 complete defluorination of PFOS and PFOA.²² Further, we demonstrated that the BN-BM process
105 outperformed BM using KOH, as evidenced by the faster PFAS destruction kinetics and higher
106 DeF. Quartz sand (SiO₂) has also been demonstrated to have reactivity in removing PFAS,
107 although < 20% defluorination efficiency was observed for PFOS and PFOA.^{19,20} Gobindlal et al.
108 used solid-state nuclear magnetic resonance (**NMR**) spectroscopy to show that insoluble Si-F
109 bonds were formed by this process, which explained the low recovery of F⁻ by solvent extraction
110 in these experiments.²¹ However, as a semi-quantitative approach, NMR analysis cannot exclude

111 the possibility that unextractable or unknown fluorocarbon residues were also formed but were
112 below the instrument detection limit or not detected using traditional analyses.

113 In this study, PFAS chemicals or undiluted AFFF (discussed later) were added to 100 mL
114 stainless steel jars filled with SS balls (16 Ø1.0 cm large balls and 100 Ø0.6 cm small balls; 160 g
115 in total) and co-milling reagents (0.4-6.0 g; details disclosed below). The planetary disk and jars
116 were rotated at 290 and 580 rpm, respectively. All BM treatment tests were conducted at room
117 temperature and atmospheric pressure.

118 **Figures 2a-c** compare the performance of BN- and SiO₂-BM processes on the destruction and
119 defluorination of 6:2 fluorotelomer sulfonate (FTS), PFOA, and PFOS. The BN-BM treatment
120 used a [BN] vs. [F on PFAS] molar ratio of 5:1, as optimized previously²², while the SiO₂-BM
121 treatment adopted a [SiO₂] vs. [F on PFAS] molar ratio of 20:1. Even though the molar dosage of
122 BN was one-fourth that of SiO₂, BN still exhibited significantly faster removal kinetics for all
123 PFAS than SiO₂ alone. BM treatment using a combination of BN and SiO₂ ([BN+SiO₂]-BM)
124 showed that the addition of SiO₂ did not promote PFAS destruction, suggesting that BN-mediated
125 destruction is the dominant mechanism in [BN+SiO₂]-BM treatment.

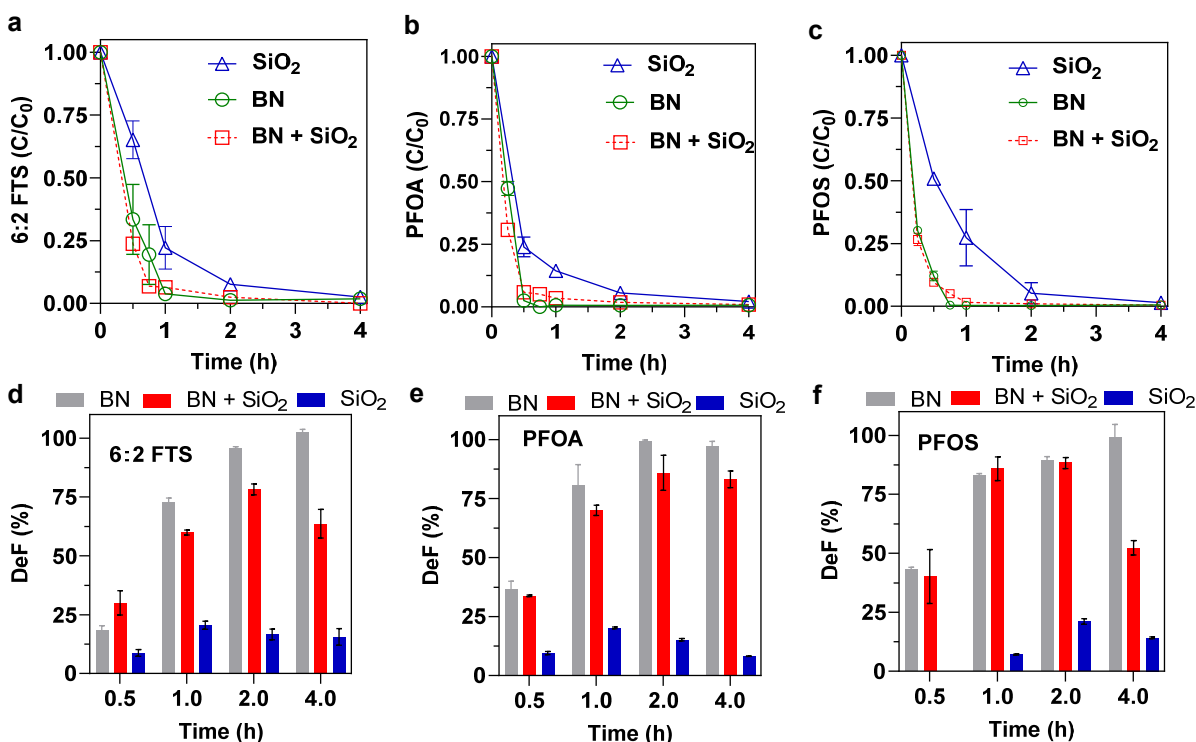
126 Previously, we reported the formation of short-chain perfluoroalkyl carboxylic acids (PFCAs)
127 intermediates in the BN-BM treatment of PFOA and PFOS.²² This study provides new
128 information for 6:2 FTS destruction. The BN-BM treatment of 6:2 FTS yielded C4-6 PFCAs
129 (**Figure S1a**). The formation of dominant intermediate perfluorohexanoic acid (PFHxA) indicates
130 the cleavage of C-C bonds of the -CF₂-CH₂- moieties. The further destruction followed the
131 -CF₂- stepwise elimination pathway to form shorter-chain PFCAs until mineralization. The
132 intermediate profiles suggest the reaction followed a series of direct electron transfer oxidation of
133 PFAS by the transient high piezoelectric potentials on BN activated by BM.²² Other aspects of the
134 reaction have already been revealed in our previous study:²² (1) BN was converted to NH₄⁺ and
135 BO₃⁻; (2) F⁻ derived from destroyed PFAS was bound by NH₄⁺ to form soluble NH₄F; (3) oxygen
136 in air-sealed in the jar is likely to be the electron acceptor in the oxidative destruction of PFAS.

137 The SiO₂-BM process may follow a different reaction pathway: BM results in the homolytic
138 cleavage of Si-O bonds in quartz to form silyl ($\equiv\text{Si}\cdot$) and siloxyl ($\equiv\text{Si}-\text{O}\cdot$) radicals,²⁶ which
139 generate $\cdot\text{OH}$ ($\equiv\text{Si}-\text{O}\cdot + \text{H}_2\text{O} \rightarrow \equiv\text{Si}-\text{OH} + \cdot\text{OH}$) and $\cdot\text{H}$ ($\equiv\text{Si}\cdot + \text{H}_2\text{O} \rightarrow \text{Si}-\text{OH} + \cdot\text{H}$) via
140 hydrolysis by moisture.^{21,27} Due to the recalcitrance of most PFAS to $\cdot\text{OH}$ attack, reductive H/F
141 exchange defluorination facilitated by $\cdot\text{H}$ is believed to be the dominant destruction pathway.^{26,28}

142 As proven in photochemical reductive defluorination studies,^{10,29} the H/F exchange followed by
143 hydrolysis or radical attack can also produce PFCAs, which explains the formation of PFCA
144 intermediates in the SiO₂-BM process (Figure S1b). Further investigation of this process was
145 beyond the scope of this study.

146 [BN+SiO₂]-BM treatment of 6:2 FTS, PFOA, and PFOS yielded PFCAs intermediates with
147 peak concentrations higher than SiO₂-BM but lower than BN-BM (Figure S1c and S2). In general,
148 BM reactions involving SiO₂ exhibited lower DeF (discussed below).

149

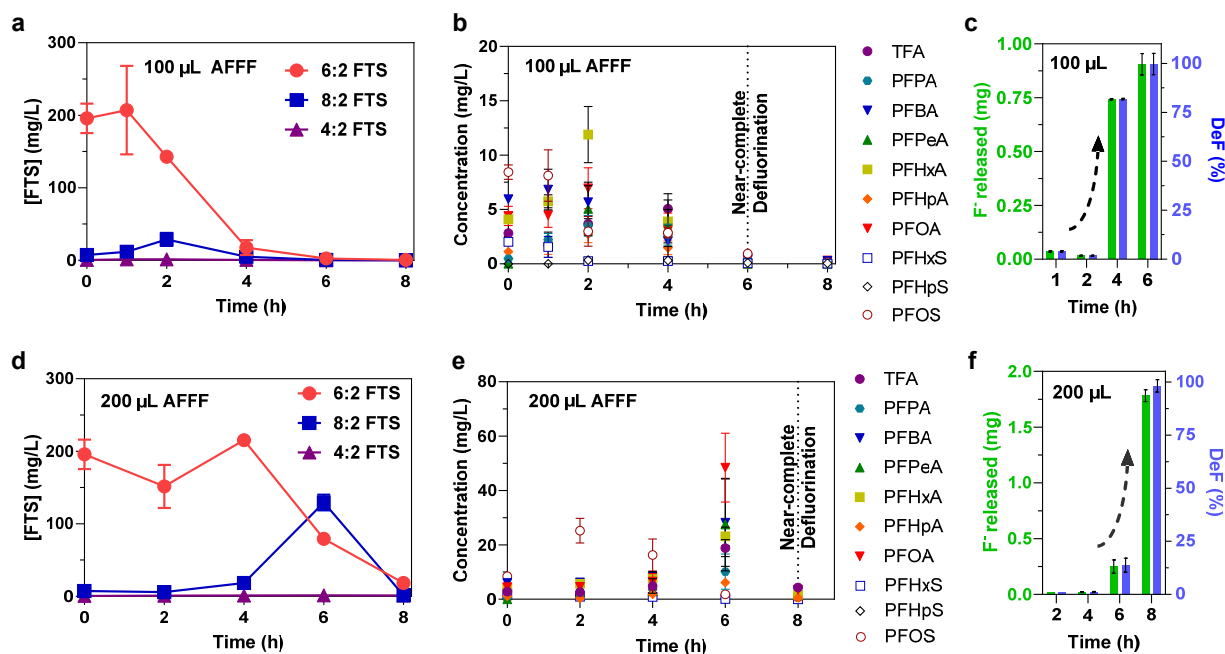


150
151 **Figure 2.** Decay of (a-c) parent PFAS and (d-f) defluorination with different co-milling reagents
152 during BM treatment. The initial mass of 6:2 FTS, PFOA, and PFOS were 0.3, 0.23, and 0.23
153 mmol, respectively. For all tests using BN and SiO₂ separately or combined, the molar ratio of
154 [BN] vs. [F on PFAS] was 5:1; the molar ratio of [SiO₂] vs. [F on PFAS] was 20:1. Data are
155 presented as mean values of triplicates ± standard deviation.

156

157 The BN-BM treatment readily achieved > 98% DeF for 6:2 FTS, PFOA, and PFOS (Figures
158 2d-f; raw data see Table S2), while less than 25% DeF was observed in experiments using only
159 SiO₂. For the [BN+SiO₂]-BM process, the DeF values were much larger than when using SiO₂

160 alone but lower than BN–BM. Moreover, DeF appeared to decrease after reaching peak values,
 161 likely because extended milling resulted in F⁻ reacting with SiO₂ to form unextractable Si–F
 162 species. Overall, these results suggest that BN is largely responsible for the PFAS breakdown to
 163 F⁻. It seems SiO₂ does not promote the BN-BM treatment of solid PFAS chemicals. However, as
 164 will be revealed below, the promotional role of SiO₂ became significant in liquid AFFF treatment.
 165
 166 **Near-complete defluorination of undiluted AFFF.**



167
 168 **Figure 3.** Time profiles of (a) FTS, (b) other PFAS, and (c) defluorination in the BM treatment of
 169 100 μ L AFFF with 0.5 g BN as the co-milling reagent. Time profiles of (a) FTS, (b) other PFAS,
 170 and (c) defluorination in the BM treatment of 200 μ L AFFF with 0.5 g BN as the co-milling reagent.
 171 The ball mill jar rotation speed was 580 rpm. Data are presented as mean values of triplicates \pm
 172 standard deviation.

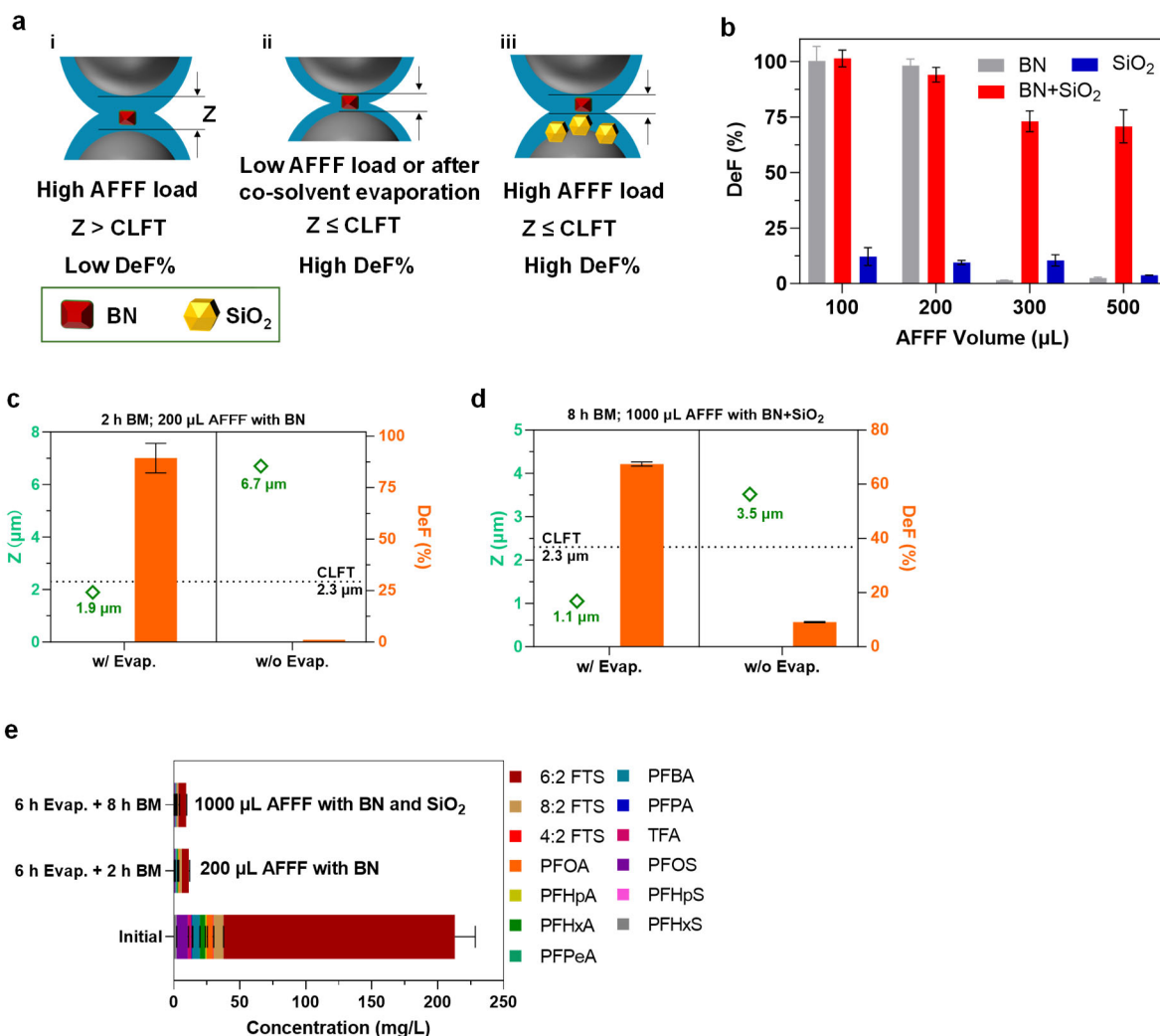
173
 174 To date, only a few studies have reported on the destructive treatment (EO, UV/S, and plasma)
 175 of diluted AFFF at ambient conditions.^{14–17,30} In those studies, the total fluorine concentrations
 176 were mostly estimated either using the total oxidizable precursor array (TOPA) analysis or NMR
 177 as 0.16–27 mg/L, and the DeF ranged from 50–81% (Table S3).

178 AFFF could be manufactured by electrochemical fluorination (ECF) or fluorotelomerization
179 (FT) methods. The manufacture of ECF-derived AFFF has been discontinued since 2002.³¹
180 Therefore, this study focused on the treatment of FT-derived AFFF, which is responsible for
181 telomer-dominant PFAS contamination in water and soil.^{5,32,33} The targeted analysis of 30 PFAS
182 in the AFFF identified 6:2 FTS (175.5 mg/L) as the dominant PFAS, along with 8:2 FTS, PFCAs,
183 and perfluorosulfonic acid (PFSAs). The TOF was 9,080 mg/L (Table S2). The fluorine on target
184 PFAS (121.7 mg/L) only makes up 1.3% of the TOF, suggesting the existence of massive amounts
185 of unidentified fluorocarbon components. The rich organic matrix contributed to an extremely high
186 total organic carbon (TOC) of 234 g/L.

187 AFFF was treated as received without dilution. Milling 0.5 g BN with 100 μ L of AFFF
188 (TOF=47.8 μ mol) led to the destruction of FTS, accompanied by the generation and decay of
189 PFCAs (Figures 3a and b). A series of $n=6-7$ PFAS surfactant precursors were detected by Q-
190 ToF-HRMS following the literature (Figure S3).¹⁸ The destruction of 6:2 FTS, 8:2 FTS, and
191 precursors via the cleavage of $-CF_2-CH_2-$ or $-CF_2-SO_2-$ followed by the hydrolysis of the
192 terminal $-CF_2\cdot$ to $-COOH$ may explain the formation of PFHxA and PFOA as intermediates.
193 Targeted PFAS and precursors were destroyed after 6 h of reaction (Figure 3a, 3b, and S3).
194 Achieving bulk defluorination (*i.e.*, all TOF broken down to F^-) of AFFF is more challenging than
195 destroying target PFAS due to the complexity of the AFFF solution. Surprisingly, after 6 h of BM
196 treatment, >99% defluorination of AFFF was achieved (Figure 3c; see Table S2 for fluorine
197 balance data). This is the very first proof-of-concept demonstrating the near complete
198 defluorination of AFFF via a novel piezoelectric BM route.

199 We further investigated the performance of the BN-BM process in treating a doubled amount
200 of AFFF (200 μ L; TOF=95.6 μ mol). Significant PFAS destruction was observed after 6 h (Figures
201 3d and e). More than 98% defluorination was still achieved after a prolonged treatment duration
202 of 8 h (Figure 3f and Table S2). These results imply that the BM process has a high robustness
203 toward AFFF loads. More importantly, it was noted that an “incubation period” was required
204 before significant defluorination (arbitrarily defined as DeF>50%). Specifically, the destruction of
205 PFAS and F^- yield abruptly accelerated after 4 and 6 h for the treatment of 100 and 200 μ L AFFF,
206 respectively. This positive correlation between AFFF loads and the incubation period was not
207 observed in the BM treatment of individual solid PFAS (Figure 2), revealing mechanistic insights
208 into the process as discussed below.

209

210 **Critical liquid film thickness.**

211
 212 **Figure 4.** (a) Schematic illustrations of the CLFT theory. (b) Defluorination efficiency (DeF) after
 213 8 h BM treatment of various volumes of AFFF. (c) Comparison of DeF and Z values of treating
 214 200 μL AFFF with or without evaporation (Evap) pretreatment using 0.5 g BN as a co-milling
 215 reagent. (d) Comparison of DeF and Z values of treating 1000 μL AFFF with or without Evap
 216 pretreatment using 0.5 g BN and 5 g SiO₂ as co-milling reagents. (e) PFAS destruction with Evap
 217 pretreatment. Evap pretreatment was performed by placing the AFFF-loaded ball mill jar in a water
 218 bath at 60 °C for 6 h with the lid open.
 219

220 As discussed in our previous study, the BM process is driven by the impact force provided by
221 ball collisions.²² In general, BM of wet media yields a lower impact force than dry BM due to the
222 presence of liquid phases that incur drag forces in the counter direction of impact.³⁴ We
223 hypothesize that due to its surfactant-like nature, AFFF should be uniformly coated on the surfaces
224 of balls and jar walls at a certain liquid film thickness (Z). Further, we propose that there is a
225 critical liquid film thickness (CLFT) so that when $Z > \text{CLFT}$ (Figure 4a-i), the drag force offsets
226 the impact force enough to retard PFAS destruction. The delivery of impact energy to BN and the
227 consequent PFAS destruction is only effective when $Z < \text{CLFT}$ (Figure 4a-ii).

228 The mechanochemical process may generate transient high temperatures at the point of
229 collision or friction.³⁵ However, the possibility of PFAS pyrolysis in our system was excluded as
230 the milling of PFAS in the absence of BN did not lead to destruction.²² The ball surface temperature
231 measured immediately after different durations of BM using an infrared thermometer was $60 \pm$
232 4 °C. This value is far below the minimum criteria (> 200 °C) of thermal decomposition of PFAS,³⁶
233 but it might be sufficient to vaporize co-solvents in AFFF. Since it is impossible to study the
234 solvent vaporization process when AFFF was blended with co-milling reagents in a fast-moving
235 jar, we placed AFFF samples in a water bath held at a constant 60°C to simulate heat-induced
236 solvent loss. The heating led to volume reduction linearly correlated with heating time (Figure
237 S4a). The 4 h heating resulted in a 38% volume reduction, and the sum of target PFAS
238 concentrations in the remaining AFFF solution increased by 37% correspondingly (Figure S4b).
239 These results indicate that heating only led to a loss of co-solvent with PFAS remaining in the
240 liquid phase.

241 Driven by the liquid film hypothesis discussed above, we took a closer look at the BN–BM
242 treatment of 100 μL of AFFF. Assuming a uniform coating of AFFF on the stainless steel balls
243 (164 cm^2) and jar walls (104 cm^2), 100 μL of AFFF in the mill should have an initial Z (Z_0) of 3.7
244 μm . Taking the data of heat-induced solvent loss measurement into consideration, a 4 h BM
245 treatment (equivalent to being heated at 60 °C for 4 h) should lead to a 38% volume reduction and
246 reduce Z to 2.3 μm . Because the steep rise in DeF was also observed at 4 h milling (Figure 3c), we
247 conclude that Z of 2.3 μm is the CLFT. The CLFT of 2.3 μm is commensurate with the sizes of
248 the BN particles at 1-2 μm (Figure S5). This observation suggests that significant defluorination
249 occurs when BN particles receive direct ball impact with minimum shielding of the liquid film
250 (Figure 4a-ii).

251 The CLFT theory can be used to explain the extended defluorination incubation period in
252 treating 200 μL AFFF. The Z_0 of 200 μL AFFF was calculated to be 7.5 μm . According to the ex-
253 situ heating tests (Figure S4), the volume reduction at 4, 6, and 8 h is projected to be 38, 56, and
254 75%, corresponding to Z values of 4.6, 3.3, and 1.9 μm , respectively. Only Z of 1.9 μm is less than
255 CLFT, which explains the sharp increase of DeF at 8 h (Figure 3f).

256 It is important to point out the caveats of the CLFT theory.

257 (1) We intentionally excluded the surface area of BN (37 m^2/g measured by N_2 -BET) in the Z
258 value calculation. This is because BN has hydrophobic surfaces.^{37,38} It cannot be completely wetted
259 by AFFF (Figure S6a). Therefore, BET surface area accessible to N_2 molecules does not represent
260 the actual effective area interacting with AFFF (which is impossible to measure experimentally).
261 This assumption also means that the Z value is a descriptor of the collision environment provided
262 by the ball milling system (jars, balls, and inert dispersants) independent of reagent properties.
263 Consequently, the model can be universally applicable to other piezoelectric co-milling reagents.
264 (2) Approximately 50% of the TOC of AFFF remained after BN-BM treatment (Figure S7),
265 indicating that the BN-BM process destroys a portion of the co-solvent, and the undestroyed
266 vaporized co-solvent was contained in the sealed jar and recondensed after the treatment. If this
267 was not the case, a more significant loss of TOC should be expected. Given a $\sim 100\%$ DeF was
268 achieved, the release of gaseous PFAS or other F-containing compounds should not be significant.
269 However, this needs to be verified in future experiments.
270 (3) The ex-situ measurement of heat-induced volume reduction (Figure S4) was performed in an
271 open system for ease of tracing weight changes and calculating the volume reduction (assuming
272 the density remained constant). In contrast, in the BM treatment, the jar was sealed, where co-
273 solvent evaporation may be inhibited by higher partial pressures than in an open system,
274 corresponding to a slower reduction of liquid film thickness. Therefore, the value of CFLT needed
275 for BM treatment may be slightly larger than that estimated above. Nonetheless, the CFLT theory
276 is sufficient to guide the process improvement.

277

278 **Promote treatment capacity based on the CLFT theory.**

279 The BN-BM process provides a novel solution to realize the near-complete defluorination of
280 AFFF at ambient conditions. Guided by the CLFT theory, we further developed two strategies to
281 promote the AFFF treatment capacity.

282 The first approach is to increase the surface area for collision. We used SiO₂ as the additive solid
283 media to augment the collision surface as it provides a hard surface (Mohs scale hardness of 7 for
284 SiO₂ and 8 for stainless steel),^{39,40} but at a much lower cost.

285 The control test using SiO₂ as the only co-milling reagent to treat 200 μL AFFF shows that the
286 target PFAS concentrations increased after BM treatment (Figure S8a). This result implies that the
287 SiO₂-BM can only break down precursors to target PFAS, while further mineralization was non-
288 existent or very slow. Consequently, the defluorination was insignificant (DeF < 10%; Figure S8b).
289 On the other hand, using BN could realize deep defluorination of AFFF, but the process failed to
290 treat AFFF at a volume higher than 200 μL (Figure 4b). Surprisingly, the BM using the
291 combination of BN and SiO₂ (e.g., [BN+SiO₂]-BM) achieved > 70% defluorination when treating
292 up to 500 μL AFFF (Figure 4b).

293 The synergy of BN and SiO₂ can be explained by the CLFT theory. As shown in Figure S6b,
294 AFFF can be dispersed on SiO₂ particles because of their hydrophilic surfaces. The SiO₂ (∅ 250
295 μm) mainly served as dispersants to provide an extra 453 cm² collision area (Text S2). When
296 amended with 5 g SiO₂, the Z₀ for treating 100 and 200 μL of AFFF are 1.4 and 2.8 μm, smaller
297 than or close to the CLFT. Therefore, efficient PFAS destruction and defluorination were
298 facilitated since the beginning of [BN+SiO₂]-BM treatment, which explains the elimination of the
299 incubation period compared with the BN-BM process (Figure S9 vs. Figure 3f). As for treating
300 300 and 500 μL AFFF with Z₀ of 4.2 and 6.9 μm, the Z's were reduced to 1.0 and 1.7 μm,
301 respectively, after 8 h of reaction. Thus, the high DeF observed at this treatment time can also be
302 attributed to Z < CLFT.

303 The second strategy to promote treatment capacity is to reduce Z₀ by pre-evaporating the
304 solvents in AFFF before BM treatment. As shown in Figure 3f, the BN-BM treatment of 200 μL
305 AFFF for 2 h led to a negligible DeF. We found that preheating the jar (lid opened) at 60 °C for 6
306 h followed by a 2 h BN-BM treatment achieved > 90% DeF (Figure 4c) and > 94% of target PFAS
307 destruction (Figure 4e). The results of these two treatment scenarios with and without pre-
308 evaporation can be explained by the CLFT theory: The heat effects of 2 h BM treatment can only
309 reduce the Z value from 7.5 to 6.7 μm, which is still larger than CLFT. Thus, the PFAS destruction
310 did not proceed effectively. However, including 6 h pre-evaporation (solvents released to air)
311 followed by 2 h BM treatment (solvents vaporized in the jar) provided an 8 h heat-induced solvent

312 loss. These approaches reduced the Z to $1.9\ \mu\text{m}$ ($<$ CLFT of $2.3\ \mu\text{m}$). Thus, a high DeF can be
313 expected for the latter scenario.

314 Last, we showcase an example of combining two strategies (i.e., introducing evaporation
315 pretreatment and increasing collision surface) to treat $1000\ \mu\text{L}$ AFFF. AFFF ($1000\ \mu\text{L}$) spiked in
316 the BN+SiO₂ system should have a Z_0 of $13.9\ \mu\text{m}$. The BM treatment without pre-evaporation
317 should reduce the Z value to $3.5\ \mu\text{m}$ ($>$ CLFT) after 8 h. Therefore, low DeF was observed at this
318 point. In contrast, a tandem process including 6 h pre-evaporation followed by 8 h BM treatment
319 incurred 14 h of heat-induced solvent loss. The Z was estimated to be $1.1\ \mu\text{m}$ ($<$ CLFT), which
320 explains the significant DeF of $>$ 60% (Figure 4d). It is of note that $>$ 90% destruction of target
321 PFAS was achieved (Figure 4e). However, SiO₂ may immobilize part of the F⁻, prohibiting the
322 treatment from demonstrating a higher DeF.

323

324 **Environmental Applications.**

325 This is the first study to demonstrate the deep defluorination of liquid undiluted AFFF by
326 piezoelectric BM at ambient temperatures and pressures. The innovation addressed the critical
327 need for non-thermal AFFF treatment. Our fundamental contribution is to identify CLFT as the
328 critical descriptor for the BM treatment of liquid waste. We present a closed-loop research
329 workflow of building the CLFT theory based on experimental data and, in return, using the theory
330 to guide the process improvement.

331 The addition of inert dispersant (e.g., SiO₂) to provide extra collision surfaces and the pre-
332 evaporation of solvents were demonstrated as two feasible options to promote AFFF treatment
333 capacity. Evaporation could be realized on commercial evaporators using waste heat or solar
334 energy. It is important to note that evaporation was introduced as an example. Other PFAS
335 concentration approaches could also be adopted. As for the BM treatment, we used 100 mL jars
336 filled with BN (0.5 g) and SiO₂ (5 g) at a balls/reagents mass ratio of 29 to treat 100-1000 μL
337 AFFF. We previously calculated that the force induced by steel ball collision in our planetary ball
338 mill is 57 N.²² These parameters lay the groundwork for the optimization and design of scaled-up
339 systems in our following studies. Should these parameters (impact force, balls to feedstock mass
340 ratio, [BN mass]/[AFFF volume] ratio, etc.) be reproduced on a commercial ball mill and the CLFT
341 criteria be met, the on-site disposal of large volume undiluted AFFF can be expected.

342 The BN–BM process shows high durability as it can destroy PFAS in the presence of extremely
343 high ~200 g/L TOC. The BN is a common commercial product. After the BM reaction, along with
344 the mineralization of organofluorine to F⁻, the reacted BN will be converted to ammonium and
345 borate.²² Even if released in the environment, BN is considered bio-compatible with non-
346 cytotoxicity.⁴¹ These unparalleled advantages empower the BN–BM process with the versatility
347 to be integrated with various water treatment trains. Given its high tolerance to organic matrices,
348 it may be able to destroy PFAS or other chemical contaminants in very concentrated waste
349 (concentrated AFFF, desalination brine, dewatered bio-solid). Given that the process is driven by
350 solid-solid phase collision, the BN–BM process is also promising for the destruction of PFAS on
351 water treatment-derived sorbents (activated carbon, ion-exchange resins, etc.). These applications
352 will be reported in our forthcoming studies.

353

354 **Methods**

355 **Chemicals and ball milling reaction.**

356 Detailed information on the chemicals used is provided in [Text S3](#). AFFF (3% AFFF Buckeye
357 MIL-SPEC) was treated as received. The BM treatment was conducted on a planetary ball mill
358 (PQ-N04, Across International).

359

360 **Solvent extraction and PFAS analysis**

361 In the tests of BM destruction of pure PFAS chemicals, the milled samples were ultrasonically
362 extracted with 50 mL of solvent (Milli-Q water for PFOA and 6:2 fluorotelomer sulfonate;
363 methanol for PFOS) for 15 min. In the treatment of AFFF, the milled sample containing co-milling
364 reagent and AFFF was extracted using 50 mL of 50% MeOH. The mixture of solvents and solids
365 was subjected to 15-min sonication and 6-min centrifugal separation at 5000 rpm. The resulting
366 supernatant (*i.e.*, extract) was then diluted to 75% methanol by 10-100 times for instrumental
367 analysis.

368 PFAS in extracts were analyzed using ultra-high-performance liquid chromatography (UPLC,
369 Thermo Vanquish) coupled to a triple quadrupole mass spectrometer (MS/MS, Thermo Altis) in
370 the Center for Air and Aquatic Research Engineering and Science at Clarkson University, a DoD
371 accredited lab for PFAS analysis. A 10 µL sample was injected and then separated on a Thermo
372 Scientific Hypersil GOLD PFP column (2.1 mm × 100 mm, 1.9 µm). Sample acquisition and

373 analysis were performed with TraceFinder 5.1 (Thermo Scientific). The setup of LC-MS/MS can
374 be found in [Text S4](#). Method detection limits of 30 PFAS were at ng/L levels, as tabulated in [Table](#)
375 [S1](#). Nontargeted analysis of PFAS precursors was conducted through a high-performance liquid
376 chromatography-quadrupole time-of-flight mass spectrometry (HPLC/QToF-MS, SCIEX) in both
377 ESI positive and negative modes. Details of the nontargeted analysis can be found in [Text S5](#).

378

379 **Analysis of F⁻, TOC, and TF.**

380 The BM-treated samples were extracted using Milli-Q water for the analyses of F⁻ and TOC.
381 F⁻ in the extracts was analyzed by a Dionex Aquion chromatography system with an anion-
382 exchange column (Thermo Fisher Scientific, RFICTM IonPacTM AS18 column). The detection limit
383 of F⁻ was 50 µg/L. Quantification of TOC was conducted on a SHIMADZU TOC-L instrument
384 that had a detection limit of 0.2 mg/L

385 The TF of AFFF was determined by combustion ion chromatography (CIC; Metrohm). AFFF
386 was diluted 500 times with Milli-Q water. Diluted AFFF (100 µL) was decomposed at 1050 °C in
387 the combustion module (Analytik Jena), and fluorine carried by argon gas was trapped by a 920
388 absorber module as F⁻, which was quantified by IC (930 Compact IC Flex). The CIC measurement
389 TF detection limit of 5 µg/L. Since no F⁻ was detected in the AFFF, the TOF of AFFF samples
390 equals their TF. Compared with other methods of TF estimation using targeted PFAS analysis (led
391 to underreporting of TF²³) and total oxidizable precursor assay (results subjected to digestion
392 conditions²⁴), CIC is the most suitable baseline for establishing a fluorine balance in this study.
393 Details of sample preparation, equipment setup, and method detection limits of F⁻, TOC, and TF
394 analyses can be found in [Text S6](#).

395

396 **Acknowledgments**

397 The authors thank the support of the U.S. National Science Foundation CAREER Award #2237080.
398 The PFAS analysis is supported in part by the U.S. National Science Foundation Award #2120452.
399 The authors thank Professor Jinyong Liu of the University of California at Riverside for providing
400 the AFFF samples. The authors thank Dr. Adarsh N. Narayanan and Professor Mario Wriedt of
401 Clarkson University for obtaining the BET surface area of BN.

402

403

404 **Data Availability**

405 The data that support the findings of this study are available within the paper and its Supplementary
406 Information. Source data for all graphs are provided with this paper. Mass spectrometry raw data
407 are available from the corresponding author upon reasonable request.

408

409 **References**

410 (1) Glüge, J.; Scheringer, M.; T. Cousins, I.; C. DeWitt, J.; Goldenman, G.; Herzke, D.;
411 Lohmann, R.; A. Ng, C.; Trier, X.; Wang, Z. An Overview of the Uses of Per- and
412 Polyfluoroalkyl Substances (PFAS). *Environ. Sci. Process. Impacts* **2020**, *22* (12), 2345–
413 2373. <https://doi.org/10.1039/D0EM00291G>.

414 (2) Evich, M. G.; Davis, M. J. B.; McCord, J. P.; Acrey, B.; Awkerman, J. A.; Knappe, D. R. U.;
415 Lindstrom, A. B.; Speth, T. F.; Tebes-Stevens, C.; Strynar, M. J.; Wang, Z.; Weber, E. J.;
416 Henderson, W. M.; Washington, J. W. Per- and Polyfluoroalkyl Substances in the
417 Environment. *Science* **2022**, *375* (6580), 16. <https://doi.org/10.1126/science.abg9065>.

418 (3) Awad, E.; Zhang, X.; Bhavsar, S. P.; Petro, S.; Crozier, P. W.; Reiner, E. J.; Fletcher, R.;
419 Tittlemier, S. A.; Braekevelt, E. Long-Term Environmental Fate of Perfluorinated
420 Compounds after Accidental Release at Toronto Airport. *Environ. Sci. Technol.* **2011**, *45*
421 (19), 8081–8089. <https://doi.org/10.1021/es2001985>.

422 (4) Hu, X. C.; Andrews, D. Q.; Lindstrom, A. B.; Bruton, T. A.; Schaidler, L. A.; Grandjean, P.;
423 Lohmann, R.; Carignan, C. C.; Blum, A.; Balan, S. A.; Higgins, C. P.; Sunderland, E. M.
424 Detection of Poly- and Perfluoroalkyl Substances (PFASs) in U.S. Drinking Water Linked to
425 Industrial Sites, Military Fire Training Areas, and Wastewater Treatment Plants. *Environ. Sci.*
426 *Technol. Lett.* **2016**, *3* (10), 344–350. <https://doi.org/10.1021/acs.estlett.6b00260>.

427 (5) Liu, M.; Munoz, G.; Vo Duy, S.; Sauv e, S.; Liu, J. Per- and Polyfluoroalkyl Substances in
428 Contaminated Soil and Groundwater at Airports: A Canadian Case Study. *Environ. Sci.*
429 *Technol.* **2022**, *56* (2), 885–895. <https://doi.org/10.1021/acs.est.1c04798>.

430 (6) Shields, E. P.; Krug, J. D.; Roberson, W. R.; Jackson, S. R.; Smeltz, M. G.; Allen, M. R.;
431 Burnette, R. P.; Nash, J. T.; Virtaranta, L.; Preston, W.; Liberatore, H. K.; Wallace, M. A. G.;
432 Ryan, J. V.; Kariher, P. H.; Lemieux, P. M.; Linak, W. P. Pilot-Scale Thermal Destruction of

- 433 Per- and Polyfluoroalkyl Substances in a Legacy Aqueous Film Forming Foam. *ACS EST*
434 *Eng.* **2023**, 3 (9), 1308–1377. <https://doi.org/10.1021/acsestengg.3c00098>.
- 435 (7) United States, Department of Defense, Office of the Assistant Secretary of Defense.
436 *Temporary Prohibition on Incineration of Materials Containing Per- and Polyfluoroalkyl*
437 *Substances (PFAS)*. [https://media.defense.gov/2022/Apr/28/2002986273/-1/-](https://media.defense.gov/2022/Apr/28/2002986273/-1/-1/1/TEMPORARY-PROHIBITION-ON-INC%5B%E2%80%A6%5DNG-PRE-AND-POLYFLUOROALKYL-SUBSTANCES-PFAS-APRIL-26-2022.PDF)
438 [1/1/TEMPORARY-PROHIBITION-ON-INC%5B%E2%80%A6%5DNG-PRE-AND-](https://media.defense.gov/2022/Apr/28/2002986273/-1/-1/1/TEMPORARY-PROHIBITION-ON-INC%5B%E2%80%A6%5DNG-PRE-AND-POLYFLUOROALKYL-SUBSTANCES-PFAS-APRIL-26-2022.PDF)
439 [POLYFLUOROALKYL-SUBSTANCES-PFAS-APRIL-26-2022.PDF](https://media.defense.gov/2022/Apr/28/2002986273/-1/-1/1/TEMPORARY-PROHIBITION-ON-INC%5B%E2%80%A6%5DNG-PRE-AND-POLYFLUOROALKYL-SUBSTANCES-PFAS-APRIL-26-2022.PDF) (accessed 2023-12-
440 12).
- 441 (8) Arana Juve, J.-M.; Wang, B.; Wong, M. S.; Ateia, M.; Wei, Z. Complete Defluorination of
442 Per- and Polyfluoroalkyl Substances — Dream or Reality? *Curr. Opin. Chem. Eng.* **2023**, 41,
443 100943. <https://doi.org/10.1016/j.coche.2023.100943>.
- 444 (9) Yang, S.; Fernando, S.; Holsen, T. M.; Yang, Y. Inhibition of Perchlorate Formation during
445 the Electrochemical Oxidation of Perfluoroalkyl Acid in Groundwater. *Environ. Sci. Technol.*
446 *Lett.* **2019**, 6 (12), 775–780. <https://doi.org/10.1021/acs.estlett.9b00653>.
- 447 (10) Bentel, M. J.; Yu, Y.; Xu, L.; Li, Z.; Wong, B. M.; Men, Y.; Liu, J. Defluorination of Per-
448 and Polyfluoroalkyl Substances (PFASs) with Hydrated Electrons: Structural Dependence
449 and Implications to PFAS Remediation and Management. *Environ. Sci. Technol.* **2019**, 53
450 (7), 3718–3728. <https://doi.org/10.1021/acs.est.8b06648>.
- 451 (11) Trang, B.; Li, Y.; Xue, X.-S.; Ateia, M.; Houk, K. N.; Dichtel, W. R. Low-Temperature
452 Mineralization of Perfluorocarboxylic Acids. *Science* **2022**, 377 (6608), 839–845.
453 <https://doi.org/10.1126/science.abm8868>.
- 454 (12) Young, R. B.; Pica, N. E.; Sharifan, H.; Chen, H.; Roth, H. K.; Blakney, G. T.; Borch, T.;
455 Higgins, C. P.; Kornuc, J. J.; McKenna, A. M.; Blotevogel, J. PFAS Analysis with Ultrahigh
456 Resolution 21T FT-ICR MS: Suspect and Nontargeted Screening with Unrivaled Mass
457 Resolving Power and Accuracy. *Environ. Sci. Technol.* **2022**, 56 (4), 2455–2465.
458 <https://doi.org/10.1021/acs.est.1c08143>.
- 459 (13) Bruton, T. A.; Sedlak, D. L. Treatment of Aqueous Film-Forming Foam by Heat-Activated
460 Persulfate Under Conditions Representative of In Situ Chemical Oxidation. *Environ. Sci.*
461 *Technol.* **2017**, 51 (23), 13878–13885. <https://doi.org/10.1021/acs.est.7b03969>.

- 462 (14) E. Schaefer, C.; Tran, D.; Fang, Y.; Jeong Choi, Y.; P. Higgins, C.; J. Strathmann, T.
463 Electrochemical Treatment of Poly- and Perfluoroalkyl Substances in Brines. *Environ. Sci.*
464 *Water Res. Technol.* **2020**, *6* (10), 2704–2712. <https://doi.org/10.1039/D0EW00377H>.
- 465 (15) Schaefer, C. E.; Choyke, S.; Ferguson, P. L.; Andaya, C.; Burant, A.; Maizel, A.; Strathmann,
466 T. J.; Higgins, C. P. Electrochemical Transformations of Perfluoroalkyl Acid (PFAA)
467 Precursors and PFAAs in Groundwater Impacted with Aqueous Film Forming Foams.
468 *Environ. Sci. Technol.* **2018**, *52* (18), 10689–10697.
- 469 (16) Singh, R. K.; Multari, N.; Nau-Hix, C.; Anderson, R. H.; Richardson, S. D.; Holsen, T. M.;
470 Mededovic Thagard, S. Rapid Removal of Poly- and Perfluorinated Compounds from
471 Investigation-Derived Waste (IDW) in a Pilot-Scale Plasma Reactor. *Environ. Sci. Technol.*
472 **2019**, *53* (19), 11375–11382. <https://doi.org/10.1021/acs.est.9b02964>.
- 473 (17) Tenorio, R.; Liu, J.; Xiao, X.; Maizel, A.; Higgins, C. P.; Schaefer, C. E.; Strathmann, T. J.
474 Destruction of Per- and Polyfluoroalkyl Substances (PFASs) in Aqueous Film-Forming
475 Foam (AFFF) with UV-Sulfite Photoreductive Treatment. *Environ. Sci. Technol.* **2020**, *54*
476 (11), 6957–6967. <https://doi.org/10.1021/acs.est.0c00961>.
- 477 (18) Hao, S.; Choi, Y.-J.; Wu, B.; Higgins, C. P.; Deeb, R.; Strathmann, T. J. Hydrothermal
478 Alkaline Treatment for Destruction of Per- and Polyfluoroalkyl Substances in Aqueous Film-
479 Forming Foam. *Environ. Sci. Technol.* **2021**, *55* (5), 3283–3295.
480 <https://doi.org/10.1021/acs.est.0c06906>.
- 481 (19) Zhang, K.; Huang, J.; Yu, G.; Zhang, Q.; Deng, S.; Wang, B. Destruction of Perfluorooctane
482 Sulfonate (PFOS) and Perfluorooctanoic Acid (PFOA) by Ball Milling. *Environ. Sci. Technol.*
483 **2013**, *47* (12), 6471–6477. <https://doi.org/10.1021/es400346n>.
- 484 (20) Turner, L. P.; Kueper, B. H.; Jaansalu, K. M.; Patch, D. J.; Battye, N.; El-Sharnouby, O.;
485 Mumford, K. G.; Weber, K. P. Mechanochemical Remediation of Perfluorooctanesulfonic
486 Acid (PFOS) and Perfluorooctanoic Acid (PFOA) Amended Sand and Aqueous Film-
487 Forming Foam (AFFF) Impacted Soil by Planetary Ball Milling. *Sci. Total Environ.* **2021**,
488 *765*, 142722. <https://doi.org/10.1016/j.scitotenv.2020.142722>.
- 489 (21) Gobindlal, K.; Zujovic, Z.; Jaine, J.; Weber, C. C.; Sperry, J. Solvent-Free, Ambient
490 Temperature and Pressure Destruction of Perfluorosulfonic Acids under Mechanochemical
491 Conditions: Degradation Intermediates and Fluorine Fate. *Environ. Sci. Technol.* **2023**, *57*
492 (1), 277–285. <https://doi.org/10.1021/acs.est.2c06673>.

- 493 (22) Yang, N.; Yang, S.; Ma, Q.; Beltran, C.; Guan, Y.; Morsey, M.; Brown, E.; Fernando, S.;
494 Holsen, T. M.; Zhang, W.; Yang, Y. Solvent-Free Nonthermal Destruction of PFAS
495 Chemicals and PFAS in Sediment by Piezoelectric Ball Milling. *Environ. Sci. Technol. Lett.*
496 **2023**, *10* (2), 198–203. <https://doi.org/10.1021/acs.estlett.2c00902>.
- 497 (23) Dubocq, F.; Wang, T.; Yeung, L. W. Y.; Sjöberg, V.; Kärrman, A. Characterization of the
498 Chemical Contents of Fluorinated and Fluorine-Free Firefighting Foams Using a Novel
499 Workflow Combining Nontarget Screening and Total Fluorine Analysis. *Environ. Sci.*
500 *Technol.* **2020**, *54* (1), 245–254. <https://doi.org/10.1021/acs.est.9b05440>.
- 501 (24) Ateia, M.; Chiang, D.; Cashman, M.; Acheson, C. Total Oxidizable Precursor (TOP)
502 Assay—Best Practices, Capabilities and Limitations for PFAS Site Investigation and
503 Remediation. *Environ. Sci. Technol. Lett.* **2023**, *10* (4), 292–301.
504 <https://doi.org/10.1021/acs.estlett.3c00061>.
- 505 (25) US EPA, O. *CWA Analytical Methods for Per- and Polyfluorinated Alkyl Substances (PFAS)*.
506 [https://www.epa.gov/cwa-methods/cwa-analytical-methods-and-polyfluorinated-alkyl-](https://www.epa.gov/cwa-methods/cwa-analytical-methods-and-polyfluorinated-alkyl-substances-pfas)
507 [substances-pfas](https://www.epa.gov/cwa-methods/cwa-analytical-methods-and-polyfluorinated-alkyl-substances-pfas) (accessed 2023-10-27).
- 508 (26) Gobindlal, K.; Zujovic, Z.; Yadav, P.; Sperry, J.; Weber, C. C. The Mechanism of Surface-
509 Radical Generation and Amorphization of Crystalline Quartz Sand upon Mechanochemical
510 Grinding. *J. Phys. Chem. C* **2021**, *125* (38), 20877–20886.
511 <https://doi.org/10.1021/acs.jpcc.1c06069>.
- 512 (27) Narayanasamy, J.; Kubicki, J. D. Mechanism of Hydroxyl Radical Generation from a Silica
513 Surface: Molecular Orbital Calculations. *J. Phys. Chem. B* **2005**, *109* (46), 21796–21807.
514 <https://doi.org/10.1021/jp0543025>.
- 515 (28) Turner, L. P.; Kueper, B. H.; Patch, D. J.; Weber, K. P. Elucidating the Relationship between
516 PFOA and PFOS Destruction, Particle Size and Electron Generation in Amended Media
517 Commonly Found in Soils. *Sci. Total Environ.* **2023**, *888*, 164188.
518 <https://doi.org/10.1016/j.scitotenv.2023.164188>.
- 519 (29) Gao, J.; Liu, Z.; Chen, Z.; Rao, D.; Che, S.; Gu, C.; Men, Y.; Huang, J.; Liu, J. Photochemical
520 Degradation Pathways and Near-Complete Defluorination of Chlorinated Polyfluoroalkyl
521 Substances. *Nat. Water* **2023**, *1*, 381–390. <https://doi.org/10.1038/s44221-023-00046-z>.
- 522 (30) Luo, Y.; Khoshyan, A.; Al Amin, M.; Nolan, A.; Robinson, F.; Fenstermacher, J.; Niu, J.;
523 Megharaj, M.; Naidu, R.; Fang, C. Ultrasound-Enhanced Magnéli Phase Ti4O7 Anodic

- 524 Oxidation of per- and Polyfluoroalkyl Substances (PFAS) towards Remediation of Aqueous
525 Film Forming Foams (AFFF). *Sci. Total Environ.* **2023**, *862*, 160836.
526 <https://doi.org/10.1016/j.scitotenv.2022.160836>.
- 527 (31) Prevedouros, K.; Cousins, I. T.; Buck, R. C.; Korzeniowski, S. H. Sources, Fate and Transport
528 of Perfluorocarboxylates. *Environ. Sci. Technol.* **2006**, *40* (1), 32–44.
529 <https://doi.org/10.1021/es0512475>.
- 530 (32) Houtz, E. F.; Higgins, C. P.; Field, J. A.; Sedlak, D. L. Persistence of Perfluoroalkyl Acid
531 Precursors in AFFF-Impacted Groundwater and Soil. *Environ. Sci. Technol.* **2013**, *47* (15),
532 8187–8195. <https://doi.org/10.1021/es4018877>.
- 533 (33) Nickerson, A.; Rodowa, A. E.; Adamson, D. T.; Field, J. A.; Kulkarni, P. R.; Kornuc, J. J.;
534 Higgins, C. P. Spatial Trends of Anionic, Zwitterionic, and Cationic PFASs at an AFFF-
535 Impacted Site. *Environ. Sci. Technol.* **2021**, *55* (1), 313–323.
536 <https://doi.org/10.1021/acs.est.0c04473>.
- 537 (34) Mori, H.; Mio, H.; Kano, J.; Saito, F. Ball Mill Simulation in Wet Grinding Using a Tumbling
538 Mill and Its Correlation to Grinding Rate. *Powder Technol.* **2004**, *143–144*, 230–239.
539 <https://doi.org/10.1016/j.powtec.2004.04.029>.
- 540 (35) James, S. L.; Adams, C. J.; Bolm, C.; Braga, D.; Collier, P.; Friščić, T.; Grepioni, F.; Harris,
541 K. D. M.; Hyett, G.; Jones, W.; Krebs, A.; Mack, J.; Maini, L.; Orpen, A. G.; Parkin, I. P.;
542 Shearouse, W. C.; Steed, J. W.; Waddell, D. C. Mechanochemistry: Opportunities for New
543 and Cleaner Synthesis. *Chem. Soc. Rev.* **2011**, *41* (1), 413–447.
544 <https://doi.org/10.1039/C1CS15171A>.
- 545 (36) Xiao, F.; Sasi, P. C.; Yao, B.; Kubátová, A.; Golovko, S. A.; Golovko, M. Y.; Soli, D.
546 Thermal Stability and Decomposition of Perfluoroalkyl Substances on Spent Granular
547 Activated Carbon. *Environ. Sci. Technol. Lett.* **2020**, *7* (5), 343–350.
548 <https://doi.org/10.1021/acs.estlett.0c00114>.
- 549 (37) Li, L. H.; Chen, Y. Superhydrophobic Properties of Nonaligned Boron Nitride Nanotube
550 Films. *Langmuir* **2010**, *26* (7), 5135–5140. <https://doi.org/10.1021/la903604w>.
- 551 (38) Yadav, V.; Kulshrestha, V. Boron Nitride: A Promising Material for Proton Exchange
552 Membranes for Energy Applications. *Nanoscale* **2019**, *11* (27), 12755–12773.
553 <https://doi.org/10.1039/C9NR03094H>.

- 554 (39) Vohera, H. *How Hard is Stainless Steel - A Complete Guide*. ThePipingMart Blog.
555 <https://blog.thepipingmart.com/metals/how-hard-is-stainless-steel-a-complete-guide/>
556 (accessed 2023-07-16).
- 557 (40) *The Mohs Hardness Scale And Chart For Select Gems*. International Gem Society.
558 <https://www.gemsociety.org/article/select-gems-ordered-mohs-hardness/> (accessed 2023-
559 07-16).
- 560 (41) Chen, X.; Wu, P.; Rousseas, M.; Okawa, D.; Gartner, Z.; Zettl, A.; Bertozzi, C. R. Boron
561 Nitride Nanotubes Are Noncytotoxic and Can Be Functionalized for Interaction with Proteins
562 and Cells. *J. Am. Chem. Soc.* **2009**, *131* (3), 890–891. <https://doi.org/10.1021/ja807334b>.
563
564